

# Number counts and redshift distribution of gravitational arclets as a probe of galaxy evolution

J. Bézecourt, R. Pelló, and G. Soucail

Observatoire Midi-Pyrénées, Laboratoire d'Astrophysique, UMR 5572, 14 Avenue E. Belin, F-31400 Toulouse, France

Received 16 July 1997 / Accepted 25 September 1997

**Abstract.** We present a detailed model of the absolute number counts, color and redshift distributions of gravitational arclets observed in clusters of galaxies. The framework adopted for galaxy evolution is chosen to reproduce the observed number counts and redshift distribution of field galaxies. Then, a spectrophotometric evolutionary code is coupled with an accurate modelling of the cluster-lens mass distribution. The interest in applying these calculations to arclets is to use cluster-lenses as filters to select faint distant galaxies, gravitational magnification being more efficient as the redshift of the galaxy is higher. This procedure is applied on two different cluster-lenses, Abell 2218 and Abell 370, for which the mass distribution is well constrained. We have studied the impact of the different sources of uncertainty on the predicted number counts and redshift distributions, taking into account the observational conditions for two sets of data, HST and ground-based images. We investigate in details the influence of the mass modelling on the counts and we show that simple cluster-scale potentials can no longer be used for arcs statistics. The main result is that arcs at redshifts between 0.5 and 1 are correctly predicted by the modelling as observed. Nevertheless, an important population of high redshift arclets ( $z \geq 1.0$ ) is also revealed by the simulations, which is not observed in spectroscopic surveys of arclets. We discuss the nature of this disagreement, due to uncertainties in the evolutionary models adopted here for galaxies at high redshift and to some biases in the spectroscopic surveys. The spatial distribution of arclets in number density and the local mean redshift of the sample are also derived. These maps can be used as a tool to optimize the search for high redshift galaxies magnified by the clusters of galaxies.

**Key words:** galaxies: cluster: individual: Abell 370, Abell 2218 – galaxies: evolution – cosmology: observations – gravitational lensing

---

## 1. Introduction

The measure of galaxy number counts and the study of the spectrophotometric properties of faint galaxies are the two

*Send offprint requests to:* J. Bézecourt, bezecour@obs-mip.fr

leading topics to constrain the evolutionary history of galaxies, a key-point of present day Cosmology. The new observational tools coming from HST imaging surveys, deep number magnitude counts in different wavelengths and spectroscopic surveys of faint galaxies have allowed to approach the spectromorphological evolution of galaxies in a reliable way. For the first time, some clues have been proposed to explain the nature of the faint blue galaxies and to determine the star formation history (see the reviews by Koo & Kron 1992 and Ellis 1997, and also Madau 1997, Metcalfe et al. 1996 and the references therein). The traditional framework for galaxy evolution cannot reproduce all the observed properties of field galaxies, namely the rapid evolution of late-type galaxies to  $z \simeq 1$ , and the lack of a dominant population of high- $z$  galaxies at  $z \geq 3$ . Different scenarios of galaxy formation and evolution have been proposed to account for observations, such as the hierarchical models (White & Frenk 1991), merging processes (Broadhurst et al. 1992), the introduction of an additional population of dwarf galaxies at  $z \simeq 1$  (Babul & Ferguson 1996) and/or the absorption of the rest-frame UV light by intervening matter (Pei & Fall 1995, Fall et al. 1996, Campos & Shanks 1995, Pozzetti et al. 1997).

Spectroscopic surveys are important tools to constrain the evolutionary scenarios, but the samples are flux limited and/or they are hardly controlled in limiting magnitudes. The surveys up to  $B = 24$  show a peak at  $z \simeq 0.5 - 0.7$  (Glazebrook et al. 1995, Cowie et al. 1996), but the lack of a large number of high redshift objects in these surveys argues for a mild luminosity evolution at intermediate redshift. From a deep sample of  $I$ -band selected galaxies, the Canada France Redshift Survey (CFRS, Lilly et al. 1995) reveals an evolution in the luminosity function (LF) of the bluer field galaxies of about 1 magnitude between  $z = 0.7$  and  $z = 0$  but fails to identify a population of high- $z$  galaxies. Spectroscopic data acquired by the Autofib Redshift Survey (Ellis et al. 1996) leads to similar conclusions about the evolution of the luminosity function with redshift and show also a clear steepening in the faint end slope of the LF. Recently, the detection of objects at  $z > 2.5$  has proved to be successful. Steidel et al. (1996a) used the Lyman dropout to photometrically identify

$3.0 \leq z \leq 3.5$  galaxies in empty fields, and they succeeded in confirming spectroscopically 16 of them at the Keck telescope. A similar technique was used on the HDF to identify at least 17 galaxies with  $2.2 \lesssim z \lesssim 3.5$ , then spectroscopically confirmed (Steidel et al. 1996b, Lowenthal et al. 1997). All these results from ground-based spectroscopy and from the HDF survey have enabled to determine the star formation rate history, which shows a maximum in the redshift range  $1 \lesssim z \lesssim 2$  (Madau 1996).

A powerful way to investigate higher redshift populations keeping the same magnitude limit is to use the gravitational magnification of background sources in the field of massive clusters of galaxies (see Fort & Mellier 1994 for a review). Serendipitously lensed by a foreground cluster, gravitational arcs and arclets are expected to be representative of the distant population of galaxies, at least up to a redshift  $\sim 1$  (Soucail et al. 1988, Pelló et al. 1991, Bézecourt & Soucail 1997, Ebbels et al. 1997), or even higher in a few cases (Mellier et al. 1991, Ebbels et al. 1996, Trager et al. 1997). Again, the limitation in magnitude for spectroscopy prevents an extensive analysis. To overcome the difficulty, several approaches are proposed, each of them being based on a redshift estimate for individual arclets. A promising one is the lens inversion technique which consists in finding the most probable redshift for each arclet, depending on its location and shape parameters, for a given lens model of the cluster potential (Kneib et al. 1994a, Kneib et al. 1996, Ebbels et al. 1997). Successfully used in a few cases, it allows to reach magnitudes up to  $B \simeq 27$  after correction for the magnification. The redshift distribution of gravitational arclets can also be estimated through multicolor photometry on a long wavelength baseline (ideally from U to K), using one of the photometric redshift techniques (Connolly et al. 1995, Pelló et al. 1996, Brunner et al. 1997). Another method consists in measuring the depletion in counts of very faint magnified sources ( $B > 26, I > 24$ ) caused by the amplification bias: depending on the slope of the number counts for field galaxies, the radial density of arclets will show a depletion curve characteristic of the redshift distribution of the sources (Broadhurst 1995, Fort et al. 1996).

The aim of the paper is to probe the spectrophotometric evolution of galaxies by computing both the number counts of arclets behind a cluster-lens and their redshift distribution. The basic idea is to consider cluster-lenses as “high- $z$  filters” which select background galaxies and distort them, making their shape easier to identify while foreground galaxies remain undistorted. Only objects with  $z$  greater than about  $2 \times z_{lens}$  can be selected with these gravitational telescopes. So the sample of arclets is a subsample of a global population of faint field galaxies in which galaxy evolution at relatively large look-back times may be much stronger. The deep number counts of arclets are then supposed to probe more directly the redshift distribution of *distant* galaxies and their relative weight with respect to a possible population of faint nearby galaxies. Previous statistical studies about the occurrence rate of arcs or arclets assumed spherical potential for all clusters and/or neglected

galaxy evolution (Nemiroff & Dekel 1989, Smail et al. 1991, Wu & Hammer 1993, Grossman & Saha 1994, Refregier & Loeb 1997, Hattori et al. 1997). The authors were more concerned about constraining the mass profile of the lenses, whereas in this paper we want to emphasize the implications on galaxy evolution. For this reason, we apply our models on real cluster-lenses (Abell 370 and Abell 2218) for which the presence of multiple-images strongly constrains the potential in the cluster core. Moreover in order to optimise the arclets identification among the crowded cluster fields, we use deep HST images available for both clusters.

This paper is organised as follows: in Section 2, we compute the number counts of gravitational arclets by combining models of spectrophotometric evolution of galaxies, which reproduce the field number-counts, and realistic models of mass distribution for clusters, which are well constrained by multiple images and giant arcs. The sensitivity of our model with respect to uncertainties on the lensing potential at large radii is tested, and the robustness of the results with respect to some observational criteria such as axis ratio or surface brightness is explored. Section 3 presents the results obtained with this method on two cluster-lenses, A2218 and A370, including a comparison between the predicted number counts of arclets and the observed ones. The sensitivity of our model to different parameters is discussed in Section 4, and some clues about the possibility to detect high- $z$  galaxies are also considered. Finally, conclusions are presented in Section 5.

Throughout the paper, we consider a Hubble constant of  $H_0 = 50 \text{ km s}^{-1} \text{ Mpc}^{-1}$ , with  $\Lambda = 0$ , and two different cosmological models corresponding to  $q_0 = 0$  and  $q_0 = 0.5$ .

## 2. Number counts and redshift distribution of gravitational arclets

The surface density of gravitational arclets obeys to two competing effects: one is the magnification of the luminosity by the cluster potential and the other one is surface dilution. If  $n(< m) = n_0 10^{\alpha m}$  is the surface density of galaxies up to magnitude  $m$  with slope  $\alpha$ , the density of arclets magnified by a factor  $M$  is

$$n_{arc}(< m) = \frac{1}{M} n(< m + 2.5 \log M) \quad (1)$$

Hence,

$$\frac{n_{arc}(\leq m)}{n(< m)} = M^{2.5\alpha - 1} \quad (2)$$

The dominating effect depends on the slope of number counts in empty fields when the mean redshift in the magnitude bin is  $z > z_l$ . For steep counts ( $\alpha > 0.4$ ), gravitational lensing will increase the surface density whereas for shallower counts a depletion will take place (Broadhurst 1995, Fort et al. 1996).

Looking in details at the number counts behind a cluster-lens, we can write the number of arclets brighter than magnitude  $m$  with an axis ratio greater than  $A_{min}$  and a surface brightness brighter than  $\mu_0$  within a given region of the sky as:

$$N(m, A_{min}, \mu_0) = \sum_i \int_{z_l}^{z_{max}} \int_{A_{min}}^{\infty} S(A, z) dA \int_{L_{min}}^{L_{max}} \Phi_i(L, z) dL \frac{dV}{dz} dz \quad (3)$$

The summation is over the different morphological types and  $z_l$  is the lens redshift.  $z_{max}(\mu_0, i)$  is the redshift cutoff corresponding to the limit in central surface brightness  $\mu_0$ .  $S(A, z, H_0, \Omega)$  is the angular area in the source plane (at redshift  $z$ ) filled by sources corresponding to arclets with an axis ratio between  $A$  and  $A+dA$ .  $\Phi_i(L, z)$  is the LF at redshift  $z$  for each morphological type.  $L_{min}(z, m, A, H_0, \Omega)$  is the luminosity of an object at redshift  $z$  which has an apparent magnitude  $m$  after magnification by the cluster, assuming that the source is circular and that its axis ratio is  $A$  after magnification (see below in Sect. 2.3). Finally,  $L_{max}$  is the bright end of the LF and  $dV(z, H_0, \Omega)$  is the volume element.

The main differences with standard number counts are: firstly, the integration in redshift runs from the lens-redshift  $z_l$  as a minimum up to a limit which depends essentially on the limitation in surface brightness  $z_{max}(\mu_0, i)$ . Gravitational lensing preserves the surface brightness of the sources, so a cut in observed surface brightness is more realistic than a cut in magnitude for extended objects. Secondly, one has to take into account the differential observed surface, computed in the source plane for each redshift and for each magnification. Finally, each luminosity has to be corrected from the magnification before the integration over the LF of the sources, as well as the minimum limit in luminosity. An additional application is to compute local values of the different parameters to derive the 2D projected number density and the mean redshift of arclets (see Sect. 3.6).

In order to validate this computation of number counts, we check first in the following section that observations in empty fields are correctly reproduced by the evolution model. We then present how to include a mass model in the problem, and the way both models are combined. We finally investigate the sensitivity of counts to these mass distributions.

## 2.1. Number counts and redshift distribution of field galaxies

### 2.1.1. Spectral energy distributions for template galaxies

As a first step, one has to define a framework for galaxy evolution that fairly reproduce both the number counts and the redshift distribution of field galaxies. We follow here the results of Pozzetti et al. (1996, hereafter PBZ) using the Bruzual and Charlot evolutionary code (1993 updated as GISSSEL95). Four galaxy types are used to represent the distribution in morphological types. They correspond respectively to an exponential star formation rate (SFR) for elliptical and spiral galaxies, with time scales of 1 Gyr and 10 Gyr for  $q_0 = 0$  (model 1) and 1 Gyr and 8 Gyr for  $q_0 = 0.5$  (model 2). A constant SFR is assumed for late type galaxies and a population of eternally young objects is also introduced by the authors to account for very blue objects. The redshift of formation for all galaxies is  $z_{form} = 4.5$  for model 1 and 5 for model 2. It should be noted that an additional assumption is made in PBZ by considering

different initial mass functions for late type spirals (Salpeter IMF, Salpeter 1955) with respect to ellipticals and normal spirals (Scalo IMF, Scalo 1986). This is necessary to obtain good fits to number counts from  $U$ -band to  $K$ -band, although the predicted colors for nearby galaxies do not match very well those observed and appear too red. A better agreement would require the use of a Salpeter IMF for all types but the drawback is that too many high redshift galaxies are produced, compared to spectroscopic surveys. Being aware of this discrepancy, we choose as prime constraints number counts and redshift distribution of field galaxies and adopt the same parameters as PBZ. A summary of the ingredients of our models is presented in Table 1. The colors for the different galaxy types at  $z = 0$  are given in Table 2, and compared to those observed in the local universe or directly derived from observed spectra (Fukugita et al. 1995).

### 2.1.2. Luminosity function

The weight affected to each galaxy type is taken from the determination of the local LF by Efstathiou et al. (1988), with the assumption that (1) morphological types are equivalent to spectroscopic types at any redshift, and (2) the weights of spectromorphological types remain unchanged with  $z$ . A model fulfilling these two conditions is a pure luminosity evolution model. Moreover, density evolution can occur due to the addition of a population of dwarf objects at low redshift or to an earlier phase of merging. A change in the overall density is not required in a low  $\Omega$  universe but it is necessary in a closed universe to reproduce number counts (Rocca-Volmerange & Guiderdoni 1990, Broadhurst et al. 1992). This is why we consider here two different models, which correspond to these two cases:

- Model 1:  $q_0=0$ , with a constant Schechter function, which is a pure luminosity evolution model.
- Model 2:  $q_0=0.5$ , a number luminosity evolution model which keeps constant the comoving mass density. The LF evolves with  $z$  according to the merging law of Rocca-Volmerange and Guiderdoni (1990):

$$\Phi_i(L, z) = (1+z)^{2\eta} \Phi_i(L(1+z)^\eta, z=0) \quad (4)$$

where

$$\Phi_i(L, z=0)dL = \Phi_i^* \left( \frac{L}{L_*(i)} \right)^{\alpha(i)} e^{-\frac{L}{L_*(i)}} \frac{dL}{L_*(i)} \quad (5)$$

is the LF at  $z = 0$  described by a Schechter law.  $i$  corresponds to each morphological type and  $\eta = 1.5$  is adjusted by Rocca-Volmerange and Guiderdoni to reproduce the field number counts.  $\Phi_i^*$  is the normalisation of the LF for each morphological type (Table 1). In the integration over the luminosities, we stop the bright end of the blue LF at  $M_{Bmax} = -23.5$  for any  $z$  in model 1, and at  $L_{Bmax}(z) = L_{Bmax}(z=0)/(1+z)^\eta$  with  $L_{Bmax}(z=0)$  corresponding to  $M_{Bmax} = -23.5$  for model 2.

Model 2 produces more faint objects at high redshift than model 1, a trend which is consistent with the results of the Autofib Redshift Survey (Ellis et al. 1996). Nevertheless, this qualitative model is somewhat unrealistic because the photometric properties induced by merging are not investigated in details. In

**Table 1.** Ingredients of the two number counts models, for two selected cosmologies.

model	$q_0$	Spectral type	fraction %	SFR	IMF	$z_f$	density evolution	$\Phi_i^*$ $10^{-3}h_{50}^3 Mpc^{-3}$	$\alpha$	$M_{B^*}$
1	0	E/S0	0.28	exp. $\tau = 1Gyr$	Scalo	4.5	no	0.95	-0.48	-20.87
		Sab/Sbc	0.47	exp. $\tau = 10Gyr$	Scalo			1.15	-1.24	-21.14
		Scd/Sdm	0.22	constant	Salpeter			0.54	-1.24	-21.14
		vB	0.03		Salpeter			0.12	-1.24	-21.14
2	0.5	E/S0	0.28	exp. $\tau = 1Gyr$	Scalo	5	yes	0.95	-0.48	-20.87
		Sab/Sbc	0.47	exp. $\tau = 8Gyr$	Scalo			1.15	-1.24	-21.14
		Scd/Sdm	0.22	constant	Salpeter			0.54	-1.24	-21.14
		vB	0.03		Salpeter			0.12	-1.24	-21.14

**Table 2.** Colors of model and observed galaxies (Fukugita et al. 1995).

type	$U - B$			$B - V$			$V - I$		
	$q_0 = 0$	$q_0 = 0.5$	observed	$q_0 = 0$	$q_0 = 0.5$	observed	$q_0 = 0$	$q_0 = 0.5$	observed
E/S0	0.70	0.63	0.45/0.40	0.99	0.96	0.97/0.93	1.61	1.56	1.45/1.25
Sab/Sbc	0.22	0.19	0.13	0.68	0.65	0.73	1.33	1.29	1.30
Scd/Sdm	-0.12	-0.14	-0.11	0.43	0.41	0.43	1.13	1.10	1.17
vB	-0.61	-0.61	—	0.01	0.01	—	0.62	0.62	—

any case, model 2 is a useful approach to the  $q_0 = 0.5$  scenario in view of the high  $M/L$  values found in weak lensing analysis (see Narayan & Bartelmann 1996 for a review) which seem to reject a low  $\Omega$  universe. Finally, the number counts of arcs and arclets are limited to redshifts higher than the lens redshift, and they are mainly sensitive to rather bright objects, even at the faintest magnitudes. For this reason, these counts do not depend severely on the uncertainties on the faint end slope of the local LF.

### 2.1.3. Surface brightness

The detection of extended objects highly depends on their surface brightness, and on the way this light is spread by seeing effects, especially on ground-based images. To include this effect in the models, we follow the observed distribution in central surface brightness  $\mu_B^0$  determined by King (1978) for ellipticals and Van der Kruit (1987) for spiral galaxies:

- E:  $\langle \mu^0 \rangle = 17.55$ ,  $\sigma = 0.15$
- S0, Sa, Sb and Sc:  $\langle \mu^0 \rangle = 21.02$ ,  $\sigma = 0.42$
- Sd and Im:  $\langle \mu^0 \rangle = 22.24$ ,  $\sigma = 0.49$

$\sigma$  being the width of the gaussian distributions.

In principle, the luminosity profile for each morphological type defines a characteristic radius which is related to the total luminosity of the galaxy,  $L(z)$ . This characteristic angular radius  $\theta$  is then convolved with the seeing to give an *observed* central surface brightness  $\mu_{obs}^0$ . A cut in  $\mu_{obs}^0$  will induce a maximum redshift at which the galaxy can be observed. This effect is

minor for elliptical galaxies because  $z_{cut} > z_{form}$  provided that the surface brightness limit is faint enough, but it should be much more sensitive for spirals. It is generally skipped in standard models of number counts of faint galaxies, but in the case of extended objects such as arclets it has to be included. For reasons of simplicity, we have adopted the crude weighting first described, with a detection limit of  $\mu_{obs}^0 = 28$  mag. arcsec $^{-2}$  in B, close to the  $2\sigma$  detection level in most of our observed images. At redshift  $z$  and for each morphological type and magnitude, a visibility weight is introduced according to the above surface brightness distributions to compute the total fraction of objects actually detected. A more realistic treatment of source profiles would require a fair knowledge of the morphological evolution of galaxies, taking into account that morphology is expected to be strongly wavelength dependent.

### 2.1.4. Results

The predictions of field number counts in the  $B$ -band are presented in Fig. 1, and the corresponding redshift distributions are shown in Fig. 2. All these calculations were performed without accounting for seeing effects. Observed number counts are taken from the compilation by Metcalfe et al. (1991) of various works. The counts at faint magnitudes were obtained by Williams et al. (1996) from the Hubble Deep Field survey. When we introduce a seeing of  $0.8''$  and a more accurate treatment of galaxy profiles, only a slight difference appears for the faintest bin in magnitude, where the counts are reduced to  $\sim 80\%$  of their value without seeing.

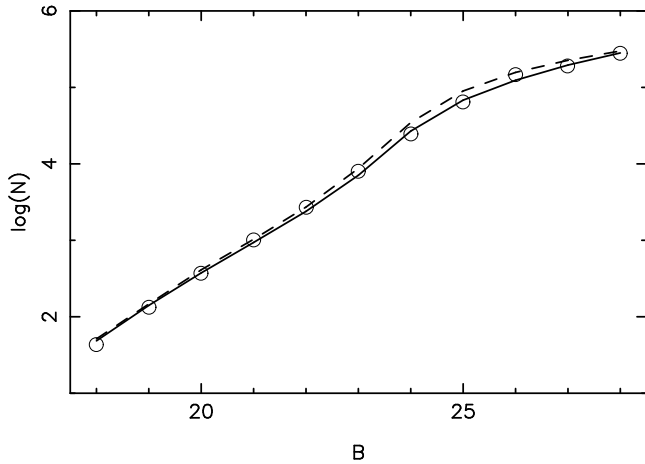


**Fig. 1.** Observed blue number counts ( $\circ$ ) (from the compilation by Metcalfe et al. (1991) completed by Williams et al. (1996)) and counts derived for model 1 (dashed line) and model 2 (solid line) per bin of one magnitude and per square degree.

We also checked that number counts in filters  $U$  and  $I$  were correctly reproduced as well as the redshift distribution of galaxies selected in  $I$  ( $17 < I < 22$ ) according to the CFRS (Crampton et al. 1995). Infrared counts in the  $K$ -band are somewhat more discrepant and show an underestimate of the counts predicted at faint magnitudes. However, our approach does not include the effects of obscuration along the line-of-sight, such as the attenuation of the starlight coming from high- $z$  galaxies by intervening matter (galaxy disks or clouds). Self-consistent models by Pei & Fall (1995) and Fall et al. (1996) have shown the importance of obscuration effects to account for the observed data on damped  $Ly\alpha$  systems, and the influence of intervening matter on the global star formation history and the cosmic chemical evolution. We are aware of this limitation in our approach, which is also common to most of the presently available models. It is worth noting that we are interested here on the effects of lensing upon individual objects and that the results by Fall et al. (1996) are insensitive to the sizes and morphologies of the damped  $Ly\alpha$  systems (disks or spheroids, the progenitors of present-day galaxies).

## 2.2. Mass distributions in clusters lenses

An accurate modelling of the mass distribution in the lens is needed because, in principle, any variation in the local substructures or in the slope of the potential may induce a change in the local magnification and axis ratio of the background galaxies. Steep surface mass density profiles will produce arclets narrower than a more gradual slope (Hammer 1991). For this reason, our model is applied on two well studied cluster-lenses, using the published lens models: Abell 370 at  $z = 0.375$  (Kneib et al. 1993) and Abell 2218 at  $z = 0.176$  (Kneib et al. 1995, Kneib et al. 1996). Both clusters are very well represented by bimodal cluster-scale mass distributions, with the clumps being centered on the two main galaxies and

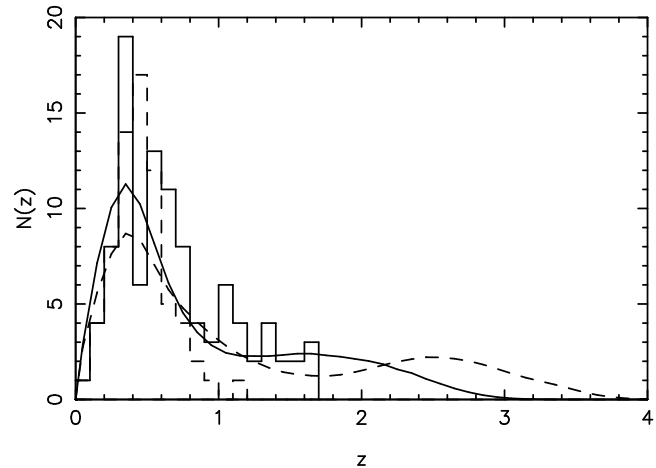


**Fig. 2.** Redshift distribution of galaxies with  $22.5 \leq B \leq 24$  for model 1 (dashed line) and model 2 (solid line). Numbers are absolute counts per bin of 0.1 in redshift, normalized to the total counts by Cowie et al. (1996). The solid histogram is from Cowie et al. (1996) data and the dashed histogram is from Glazebrook et al. (1995). Models predict  $\sim 20\%$  of the total number counts at  $z \geq 1.5$ .

the potentials modelled by pseudo isothermal elliptical distributions (PIEMD, Kassiola & Kovner 1993). In the improved modelling for A2218 (Kneib et al. 1996), the authors introduce an additional galaxy-scale component in the mass distribution. Each one of the 34 brightest cluster galaxies is modelled by a pseudo-isothermal elliptical mass distribution with the parameters (truncation radius, core radius and velocity dispersion) scaled to the galaxy luminosity. The effect on number counts of uncertainties in the mass distribution is quantified below (see Sect. 2.5).

## 2.3. Axis ratio and magnification

$S(A, z)$  in equation (3) is the background surface at redshift  $z$  where the sources have an axis ratio between  $A$  and  $A + 1$  after magnification. It is a specific term related to lensing and magnification, which makes the arclet number counts quite different from results in empty fields. Numerically,  $S(A, z)$  is obtained by computing the area in the image plane where arclets with  $A \leq a/b \leq A + 1$  can be found, and then dividing by the magnification at each point because of the dilution factor in the image plane. The upper limit chosen for the magnification is 20, a value representative of giant arcs, but of negligible effect because statistics is not dominated by giant arcs. In practice, as number counts will be computed in the image plane, we have chosen to scan this plane with a grid of  $1''$  step and then to relate these image elements to the corresponding surface in the source plane at each redshift.

The relation between the axis ratio and the magnification of an arclet is not unique for the complex lens potentials we use in the model and varies locally (see Bartelmann & Weiss 1994 for an illustration). For each arclet, the observed axis ratio is the result of the intrinsic size of the source ( $\theta_{hl}$ , half light angular

radius), tangential and radial magnifications ( $\lambda_t$ ,  $\lambda_r$ ) and seeing ( $s$ ):

$$\frac{a}{b} = \sqrt{\frac{(2\lambda_t\theta_{hl})^2 + s^2}{(2\lambda_r\theta_{hl})^2 + s^2}} \quad (6)$$

All sources are considered circular because it is not worth introducing an ellipticity distribution when we are only interested in arclets with rather high axis ratio ( $a/b \geq 2$ ), and when the intrinsic ellipticity is negligible compared to the one induced by the lens. However, we are aware of the higher importance of source ellipticities in weak lensing studies, when reconstructing mass profiles.

We have investigated the influence of the size of the sources through two additional hypothesis: a) the linear size is constant (models 1a and 2a, for  $q_0 = 0$  and  $q_0 = 0.5$  respectively), and b) the linear size decreases with  $z$  (models 1b and 2b, for  $q_0 = 0$  and  $q_0 = 0.5$ ). The former set of models apply a linear size of 8.7 kpc to the half light radius of the sources, a typical value for nearby spiral galaxies (Mathewson et al. 1992), also compatible with the Medium Deep Survey results (the MDS project) which show a rather constant size for galaxies up to  $z \simeq 0.8$  (Mutz et al. 1994). The second set of models is motivated by the results of lens inversion by Smail et al. (1996), based on HST images, according to which the half light radius of the sources of giant gravitational arcs follows approximately the relation  $r_{hl} \propto 1/(1+z)$ . This law is also in good agreement with the typical sizes observed for the most distant galaxies (Trager et al. 1997, Lowenthal et al. 1997).

#### 2.4. Surface brightness and seeing effects

For number counts of arclets, the effect of seeing is important because it modifies the shape of the images. Although gravitational lensing does not change the surface brightness, an arclet appears larger than the equivalent unlensed galaxy, and its luminosity profile is stretched. Hence flattening by the seeing is less effective for a lensed object than for its source galaxy. In addition to simple magnification, gravitational lensing makes the detection of faint galaxies easier by increasing their mean surface brightness. This effect can be approximated by considering the change in surface introduced by the seeing:

$$\mu = \mu(\text{no seeing}) - 2.5 \log \frac{ab}{\sqrt{(a^2+s^2)(b^2+s^2)}} \quad (7)$$

where  $a$  and  $b$  are the semi major and semi minor axis of the arc and  $s$  is the seeing FWHM. In the case of HST data,  $s$  is equal to 0.1'' although data are undersampled by the pixel size. The result is also sensitive to the way  $a$  and  $b$  are measured, the central part being more circular than the limiting isophote after convolution. We choose here to consider the half light distances in both axis. A more precise treatment is proposed by Hattori et al. (1997) who consider isophotal magnitudes whereas we are concerned here with total magnitudes, less sensitive to detection conditions. In the following we limit the counts to arcs with central surface brightness  $\mu_B^0 < 26.5$  or  $\mu_R^0 < 25.5$ .

#### 2.5. Sensitivity to the mass distribution

We check here the sensitivity of our model to uncertainties on the mass distribution. In particular, we focus on the effects of varying the assumptions for the cluster potential in the two cluster-lenses considered.

As explained in Sect. 2.2, two lens models are available for the cluster A2218 (Kneib et al. 1995 and Kneib et al. 1996): the first one with only cluster-scale mass components, and the improved one with 34 additional galaxy-scale components in the mass distribution. Both of them reproduce correctly the observed shear pattern. Nevertheless, the second model increases the local magnification and distorts the critical lines in the regions around each lensing galaxy, in such a way that a lensed image located in this area will be divided in 2 or 3 parts whereas the same object would appear as a giant arc with a smoother cluster-scale potential. Hence a higher number of arclets is expected, for a given set of lens parameters. This point is crucial in our problem because although they do not dominate the arcs counts, multiple images can distort our statistics of small numbers, at least in a few magnitude bins.

The uncertainty introduced by the slope of the cluster potential in the external part of the deflector, where most of the arclets appear, has also been investigated with the lens model of A370. In this case, the mass distribution in the central part of the cluster is very well constrained by two systems of multiple images (Kneib et al. 1993). Hence, we have introduced modifications in the external potential only, keeping the center unchanged. The external region is defined by a limiting ellipse oriented parallel to the line linking the two central galaxies and with a semi major axis of 40''. Inside the ellipse we keep the potential to the expression by Kneib et al. (1993):

$$\phi(r, \theta) = \phi_{G20}(r, \theta) + \phi_{G35}(r, \theta) \quad (8)$$

where G20 and G35 are the main cluster galaxies (see Mellier et al. 1988). Outside the ellipse, the potential is not bimodal any longer but it follows the same law as for each clump, characterized by an ellipticity  $\epsilon$ , a velocity dispersion  $\sigma$ , a core radius  $r_c$ :

$$\phi(r, \theta) = \phi_0 \left[ \sqrt{1 + \left(\frac{r}{r_c}\right)^2} + \frac{\epsilon \left(\frac{r}{r_c}\right)^2 \cos(2(\theta - \theta_0))}{\sqrt{1 + \left(\frac{r}{r_c}\right)^2}} \right]^\gamma \quad (9)$$

$\gamma$  is a parameter which characterizes the slope of the potential, and  $\phi_0 = 6\pi \left(\frac{\sigma}{c}\right)^2 r_c \frac{D_{ls}}{D_s}$ . Note that this potential is continuous only along the major axis of the limiting ellipse, but this simplification is used to test the effects of the potential slope on the absolute normalisation of arcs number counts. Outside the ellipse, the parameters of the global potential are  $\gamma = 1$ ,  $\epsilon = 0.38$ ,  $r_c = 20''$  and  $\sigma = 1000 \text{ km s}^{-1}$  to fit the modelling of Kneib et al. (1993). The values  $\gamma = 0.8$  and  $\gamma = 1.1$  have been chosen to provide respectively an underestimate and an overestimate of the surface mass density of 20% at large distance from the center of the cluster (Fig. 3). Such fluctuations in the mass density correspond to variations in the parameters far beyond the published uncertainties. Whatever the model used, we have checked that

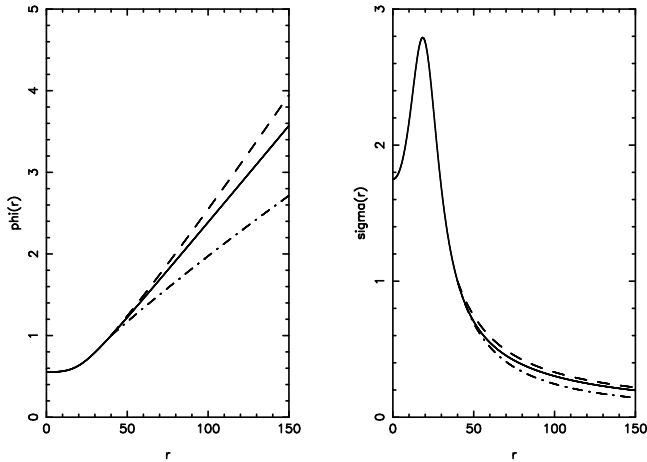


**Fig. 3.** Gravitational potential (left) and surface mass density (right) along the line G20 – G35 in A370. Solid lines are for the expression given in Kneib et al. (1993); also shown are the cases:  $\gamma = 1.1$  (dashed line) and  $\gamma = 0.8$  (dot-dashed line).

the change in the amount of mass in the external parts of the cluster-lens simply scales the total number of arcs seen through a cluster, with a similar shape for the redshift distribution (*i.e.* an overestimate of the total mass,  $\gamma=1.1$ , increases the number of arclets by 25% while an underestimate,  $\gamma=0.8$ , will decrease it by 30%).

### 3. Results

#### 3.1. Catalogs of observed arclets

The detection of elongated objects in the two cluster-lenses was performed in the frame of WFPC2 HST images, obtained from the STScI Archives: 5600 sec of exposure in filter F675W for A370 (P.I.: R.Saglia), and 6500 sec of exposure in filter F702W for A2218 (Kneib et al. 1996). The  $B - F702W$  color distribution of arclets in A2218 is also studied below. Blue magnitudes for A2218 were determined from ground-based deep B images obtained at the 3.5m telescope at Calar Alto (Pelló et al. 1992). The pixel size was  $0.25''$  and the seeing was  $1.1''$  in this case.

The SExtractor package (Bertin & Arnouts 1996) was used to detect the arclets, with the requirement for an object to have at least 12 contiguous pixels above  $2\sigma$  of the local sky level. The  $1\sigma$  detection limit is  $R \simeq 25.2$  mag. arcsec $^{-2}$  in A2218 and  $R \simeq 24.9$  mag. arcsec $^{-2}$  in A370. We limit the sample to objects with total  $R$  magnitude between 21.5 and 25.5 and axis ratio greater than 2, the bright end cut is aimed to avoid contamination by cluster members. A close inspection of each object has been done to eliminate objects with problems in detection or photometry (close or inside the PC, partially out of field,...), and also those showing position angles outside the range  $\pm 45^\circ$  from the predicted local shear. The final catalog contains 73 objects in A2218 and 81 objects in A370, the number of objects excluded on the basis of a wrong position angle with respect to the shear direction being 2 and 12 respectively.

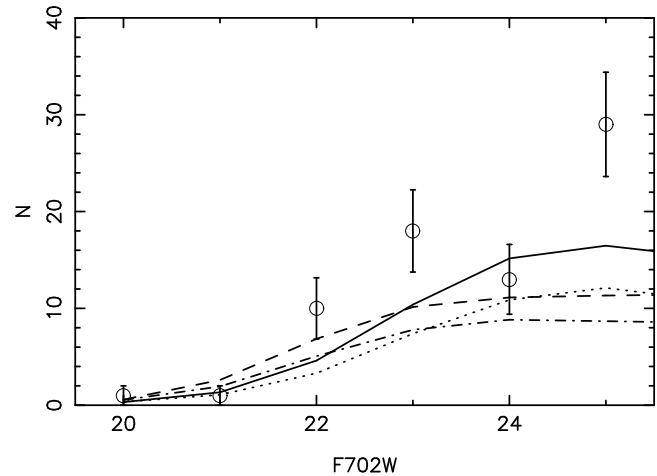


**Fig. 4.** Number counts of arclets in A2218 with the F702W filter, per bin of one magnitude, up to  $R_{F702W}=25$ . Selection criteria are:  $a/b > 2$  and  $\mu_{F702W}^0 \leq 25.5$ .  $\circ$ : observed counts. The solid line corresponds to  $q_0 = 0.5$  (model 2a) and the dashed line to  $q_0 = 0.0$  (model 1a), both computed through the lens model by Kneib et al. (1996). The results obtained with the cluster-scale mass distribution only (Kneib et al. 1995) are also displayed for comparison: dotted line and dot-dashed line correspond to count models 2a and 1a respectively. No evolution in the source size has been included as it does not change the graphs (see text for more details). Errors bars correspond to statistical fluctuations.

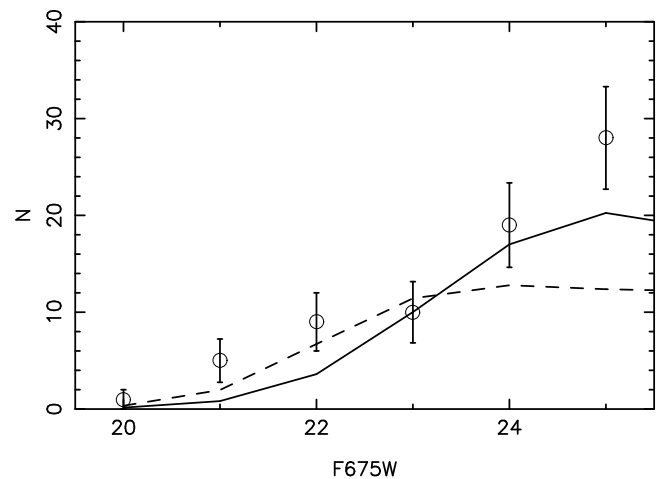


**Fig. 5.** Number counts of arclets in A370 with the F675W filter, per bin of one magnitude. Selection criteria are:  $a/b > 2$  and  $\mu_{F675W}^0 \leq 25.5$ . Same notations as in Fig. 4.

#### 3.2. Absolute number counts

The observed and predicted number counts of arclets versus  $R$  magnitude in A2218 are shown in Fig. 4. The predicted total number of arcs ( $R_{F702W} \leq 23.5$  and  $a/b \geq 2$ ) with the best mass model is lower than the observed number by a factor of 2 (table 3). Similar counts in A370 with  $a/b \geq 2$  are displayed in Fig. 5. Again, the models underpredict the observed counts by a factor of  $\sim 1.3$  at the faintest magnitudes. The contamination by cluster members is possible, especially for the less elongated

**Table 3.** Comparison of different mass models for A2218 from Kneib et al. 1995 and Kneib et al. 1996. Number of arclets with  $R \leq 23.5$  and  $\mu_R \leq 25.5$  in the frame of the HST image for model 2a, compared to the observations.

mass model	$a/b \geq 2$	$a/b \geq 3$
bimodal (Kneib et al. 1995)	12.1	5.1
multimodal (Kneib et al. 1996)	16.7	7.9
observed arclets	30	13

objects or the faintest ones. The number of objects excluded in each cluster allows to estimate this source of contamination, which is unable to explain all the observed excess. Some clues to understand this discrepancy in terms of cosmological parameters, LF and clustering are given in Sect. 4.

### 3.3. Color distributions

Another test of reliability for these results is to compare the predicted with the expected color distribution of arclets. To do that, the evolution with  $z$  of the color index  $B - F702W$  was computed for the four morphological types of galaxy included in the model. Then, these discrete values were replaced by a gaussian distribution for each type ( $\sigma = 0.15$  mag.) and the counts in color were computed in the usual way. These predictions have been compared to the observed values in A2218. Because of the different detection conditions in the  $B$ -band compared to the WFPC2 (exposure time, seeing, pixel size), the resulting catalogue is limited to 49 objects with  $B < 27.0$  and  $a/b > 2$ , 21 of them at  $B < 24.5$ . The color distribution of arclets in A2218 for  $R_{F702W} \leq 25.5$  and  $a/b \geq 2$  is shown in Fig. 6. The observed range of  $B - F702W$  is well reproduced by the models, although the modelled colors tend to be slightly bluer than observed. This effect is probably due to the way color indices are computed on CCD images: with such different sampling and observing conditions, colors are obtained roughly as the difference between the measured magnitudes, HST magnitudes being total ones while B-magnitudes are isophotal. As isophotal magnitudes tend to be overestimated at faint fluxes, the net effect is an artificial reddening of the sample which could explain this small discrepancy.

### 3.4. Redshift distributions

For a direct comparison with existing deep redshift surveys, the redshift distribution of arclets has been computed in both  $B$  and  $R$  filters. These results are shown in Figs. 7 and 8 for A2218, and in Fig. 9 for A370. In the case of A2218, our results can be partially compared to the results of a successful spectroscopic survey of arclets (Ebbels et al. 1997), where 19 redshifts were obtained ranging from  $z = 0.45$  to 2.5, and observed magnitudes from  $R = 20.0$  to  $R = 23.5$ . This observed distribution peaks to a mean value of  $\langle z \rangle = 0.7$ , with only two objects

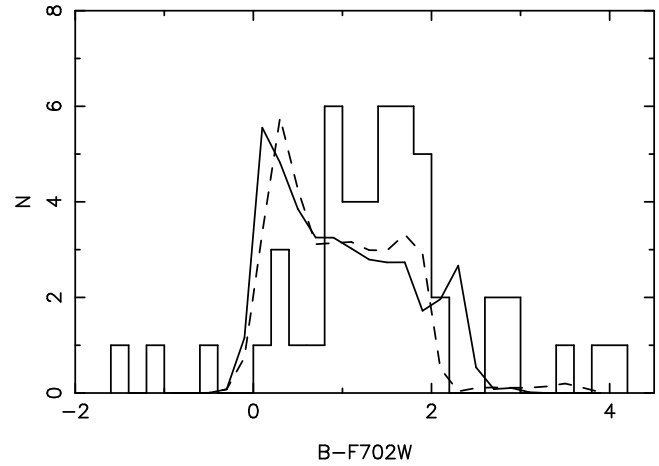


**Fig. 6.** Color distribution of arclets in A2218 with  $R_{F702W} < 25.5$  and  $a/b > 2$  (mass modelling by Kneib et al. (1996)) for model 1a (dashed line) and model 2a (solid line). The histogram is the observed color distribution. The reddest observed overdensity may be due to some cluster contamination ( $B - F702W \simeq 2.0$  for elliptical galaxies at the cluster redshift).

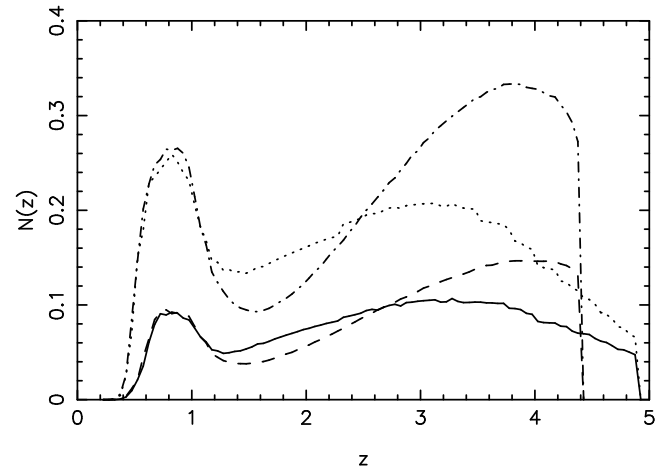


**Fig. 7.** Redshift distribution of arclets in A2218 per bin of 0.05 in  $z$ , in the HST field ( $R_{F702W} \leq 23.5$  and  $\mu_R \leq 24$ ) for  $q_0 = 0$  (dot-dashed line:  $a/b > 2$ , dashed line:  $a/b > 3$ ) or  $q_0 = 0.5$  (dotted line:  $a/b > 2$ , solid line:  $a/b > 3$ ).

at  $z > 1$ . Fig. 7 shows the redshift distribution of arclets expected with the same selection conditions than that adopted by Ebbels et al. 1997. The peak observed is remarkably well reproduced. However, another population of objects is expected at higher redshifts,  $z > 2$ , with models 1 and 2, which is not seen in these data. This high redshift tail is mainly produced by elliptical-type galaxies and it is sensitive to the redshift of formation assumed for the sources and to the hypothesis of no-evolution in morphological types. The maximum value of  $N(z)$  at  $z > 2$  is lowered by 30 – 50% assuming a redshift of formation  $z_f \sim 6$ , but the distribution extends to higher redshifts keeping the total number of objects approximately constant. Selection biases affecting the spectroscopic sample, the accuracy

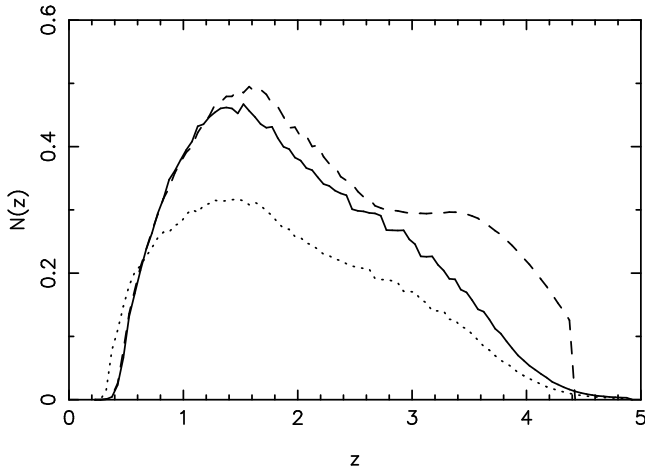


**Fig. 8.** Redshift distribution of arclets in A2218 per bin of 0.05 in  $z$ , with  $B \leq 24.5$  and  $a/b \geq 2$ , according to the mass distribution by Kneib et al. (1996) for model 1a (dashed line) and model 2a (solid line). Dotted line corresponds to the bimodal mass distribution of Kneib et al. (1995) for model 2a. The cut at  $z = 4.5$  corresponds to the redshift of formation for  $q_0 = 0$ .

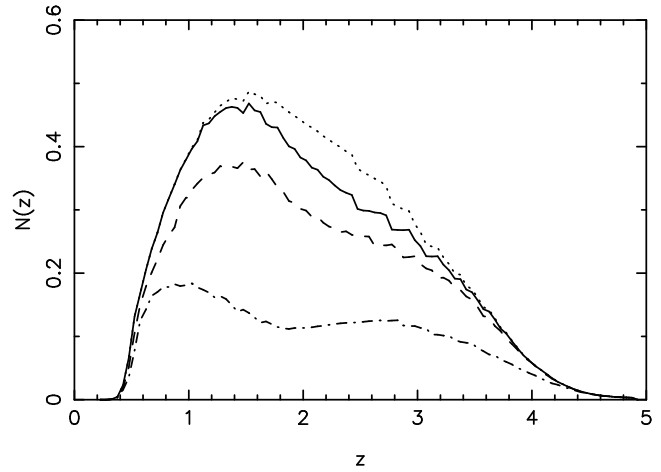


**Fig. 10.** Redshift distribution of arclets in A2218 per bin of 0.05 in  $z$  ( $B \leq 24.5$ ,  $a/b \geq 2$  and  $\mu_B^0 \leq 26.5$ ). Solid line is for no seeing, dashed line corresponds to a seeing of  $1''$  while dotted line corresponds to no seeing and no threshold in surface brightness, all curves are for model 2a. Dot-dashed line corresponds to model 2b with a seeing of  $1''$  (evolution of the source size).

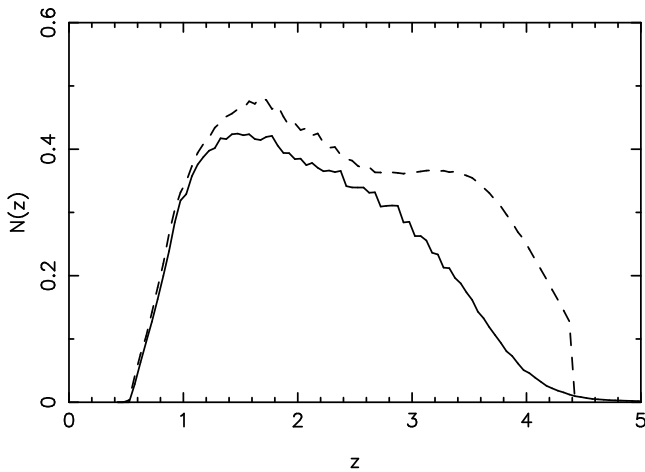


**Fig. 9.** Redshift distribution of arclets in A370 per bin of 0.05 in  $z$  ( $B \leq 24.5$  and  $a/b \geq 2$ ) for model 1a (dashed line) and model 2a (solid line). The cut at  $z = 4.5$  corresponds to the redshift of formation for  $q_0 = 0$ .

of the lens model and the effects of clustering behind the lens are discussed below (Sect. 4).

We have also tried to compare our model with a larger sample of giant arcs and arclets originating from different clusters (Fig. 11), from a compilation of all measured redshifts at the present day. Again, in this sample arclets are mostly found between  $z=0.5$  and 1, although arcs produced by different mass distributions are mixed and cannot be used for a close comparison with Fig. 8. This sample is however interesting because it corresponds to arcs with high magnifications so the integrated flux favours the acquisition of better S/N ratio on the continuum of the spectra. Some absorption lines are expected to be

observed at least in a few cases of star forming galaxies, and they would help in principle to determine redshifts in the range  $1.2 \leq z \leq 2.2$  where no emission lines are present in the visible spectrum. This may be the case for the giant arc in Cl0024+17 (Mellier et al. 1991) where a blue continuum is detected with no emission lines, but no firm identification has been proposed up to now. Being aware that objects with  $1.2 \leq z \leq 2.2$  are systematically missed in spectroscopic surveys because of the lack of strong spectral features in their visible spectrum, we find again a similar trend: present-day arcs spectroscopy reveals very few objects at  $z > 2$ , whatever the selection criteria are.

### 3.5. Size evolution of sources

When neither the seeing nor the surface brightness are considered, the total number counts and the color distributions of arclets are almost independent of the size evolution of sources with redshift. On the contrary, when realistic ground-based detection conditions are introduced in the model, the resulting redshift distribution can differ significantly. Fig. 10 shows these effects on the redshift distribution of arclets in A2218. When an atmospheric seeing of  $1''$  is introduced together with size evolution of galaxies, the observed population splits into two components: one corresponds to spirals at redshifts of the order of 1 and the other one to ellipticals at  $z$  greater than 2. The former probably constitutes the bulk of the redshifts compiled in Fig. 11 because most of these arcs were selected on ground based images and display emission lines. As expected, including an evolution of the size of galaxies does not change the results on HST data where the PSF is always smaller than the angular size of the sources whatever the redshift.

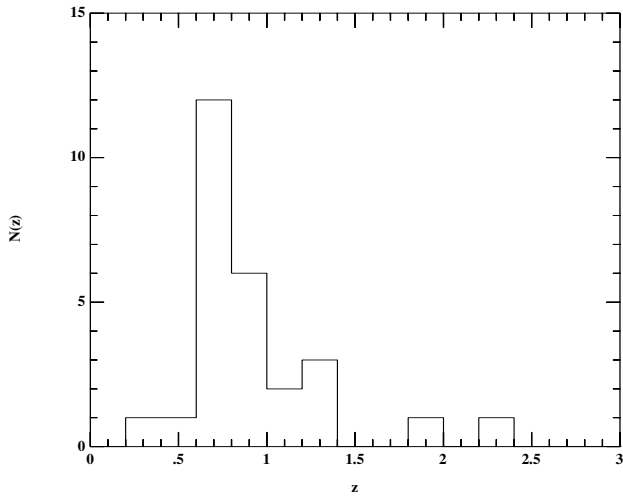


**Fig. 11.** Redshift distribution of arclets in several clusters except A2218. References: Soucail et al. 1988 (A370), Mellier et al. 1991 (A370 and Cl2244–02), Fort & Mellier 1994 (A2163 and S295), Pelló et al. 1991 (A2390), Bézecourt & Soucail 1997 (A2390), Melnick et al. 1993 (Cl2236–04), Kneib et al. 1994b (Cl2236–04), Smail et al. 1995 (AC114), Ellis et al. 1991 (A963), Lavery et al. 1993 (GHO2154+0508), Allen et al. 1996 (PKS0745).

### 3.6. Optimisation of the search for high- $z$ galaxies

One of the most interesting issues of this work is to produce a tool to select lensed galaxies at various redshifts. Instead of computing counts in the whole field, one can compute the 2D distribution for both counts and mean redshifts, in order to estimate and to compare the local densities all over the field. For computational reasons, the surface brightness distribution in Sect. 2.1.3 was replaced by the mean value of  $\mu_B^0$  for each morphological type. The results for A2218 are shown in Fig. 12. The area where arclets are observed is fairly well identified (see Fig. 1 in Kneib et al. 1996 for comparison). These figures show the places where the numerous high redshift objects (seen in the  $N(z)$  curves) are expected. As one goes away from the cluster center, only arcs with high  $z$  can be lensed to acquire an axis ratio greater than 3. However, in the limiting area where arcs can be found, the cutoff in the density of arcs is quite sharp. In the very center of the cluster, radial arcs at high redshift are also predicted by the model. These objects remain unobserved because of obscuration by the cD envelope.

With the help of our model and maps similar to those in Fig. 12 we can optimize the search for well defined samples of arclets and/or the search for high redshift lensed galaxies. The selection procedure could even benefit from the combination with redshifts estimated through multi-color photometric techniques (Connolly et al. 1995, Pelló et al. 1996, Brunner et al. 1997) or with the so-called “lensing redshift” (Kneib et al. 1994a, Kneib et al. 1996). Note that some high- $z$  lensed galaxies at  $z \geq 4$  have already been detected, although serendipitously, in the cluster Cl0949+4713 (Trager et al. 1997), or in Cl1358+62

(Franx et al. 1997), all of them showing “red” colors in the visible.

## 4. Discussion

### 4.1. Number counts of arclets

The observed absolute number counts of arclets presented in Figs. 4 and 5 tend to be overestimated with respect to the predicted values, especially at faint magnitudes where the excess attains a factor of 1.3 to 2. Computing number counts is difficult because of the large number of uncertainties involved in models. Some of them concerning the evolution of galaxies are quite similar to those encountered in empty fields. For example, number counts depend on the local normalisation of the LF, which has an uncertainty of a factor of 2 (see the discussion in Ellis et al. 1996), due to the statistical fluctuations from field to field and to the clustering of background galaxies. These fluctuations may also introduce a bias because we are looking deeply at only a few lines of sight, and the cluster-lenses selected at first are among those with the highest number of arcs and arclets. This last bias is difficult to avoid, but is not expected to induce an excess larger than a factor of 2. A possible excess of galaxies at  $z \simeq 0.45$  is indeed mentioned by Ebbels et al. (1997) in A2218 but it does not seem to strongly distort the final redshift distribution. Another example of clustering of background galaxies is observed behind the cluster-lens A2390, where two redshift planes are suspected behind the cluster (Bézecourt & Soucail 1997).

Anyhow, a spectacular change in the number counts is obtained when we take into account the effects due to galaxy-scale mass components. The number of lensed objects is increased thanks to both the local enhanced magnification and the additional critical lines which divide giant arcs in smaller ones. We illustrate this effect in Sect. 3.2 and Sect. 3.4 in the case of A2218, where the number of arclets is a factor of 1.5 higher when galaxy-scale mass components are introduced. This is a strong justification for an accurate modelling of the lens when computing arcs statistics, and in this sense the present model is a clear improvement with respect to previous similar works (Nemiroff & Dekel 1989, Grossman & Saha 1994). The absolute normalisation of counts through a cluster-lens has been approached in a reliable way for A2218. In the case of A370, the lens modelling has to be improved by adding the local effects of individual galaxies as additional mass components. This is a work in progress thanks to the constraints given by new spectroscopic results which clearly confirm some multiple image candidates. The results will be presented in a forthcoming paper. They confirm the increase of the predicted number of arclets and may reconcile the observed number of arclets presently in excess with model predictions for this cluster.

Another major point to discuss is the sensitivity of our results to the geometry of the universe. The two models considered here have been fixed to reproduce both number counts and redshift distributions of galaxies in the field. The mass models used in all the simulations were determined for a universe with  $\Lambda = 0$

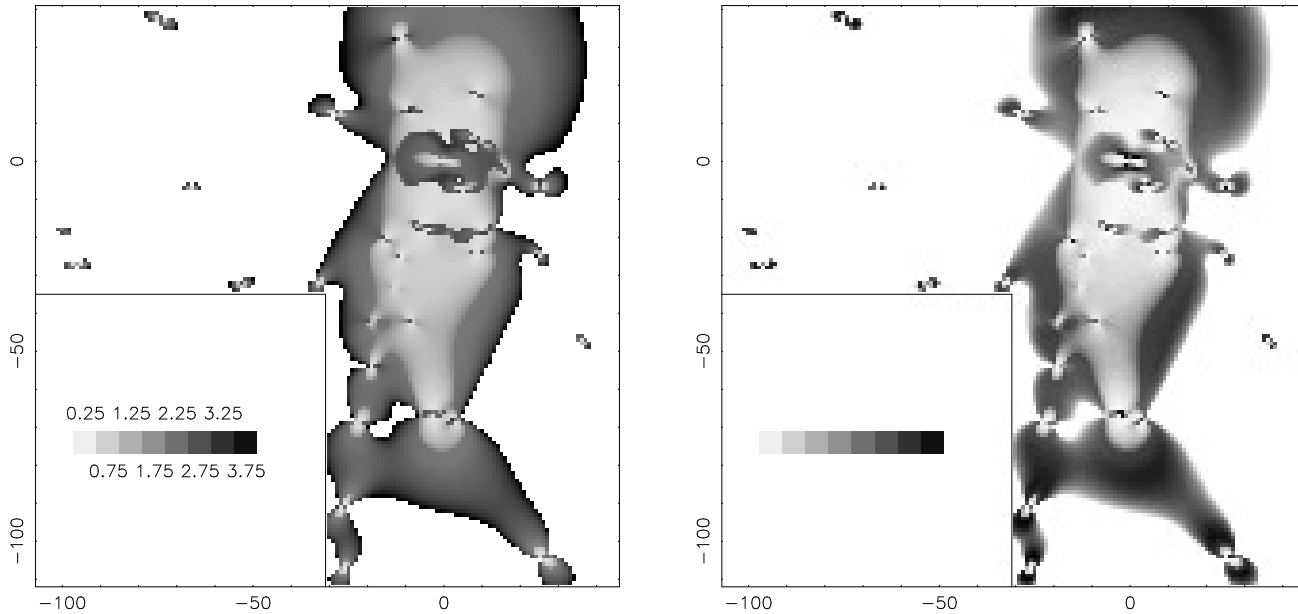


**Fig. 12.** Left: Density of arclets in cluster A2218 with  $B < 24.5$  and  $a/b > 3$  for model 1a. The arclets density increases from white pixels (null density) to black pixels. Right: Mean redshift of arclets in cluster A2218 with  $B < 24.5$  and  $a/b > 3$  for model 1a. Gray scale levels corresponds to redshift bins of  $\Delta z = 0.5$  from  $[0.0, 0.5]$  (clearer pixels) to  $[3.5, 4.0]$  (black pixels).

and  $\Omega = 1$ . It was assumed here that the same models were still valid for  $\Omega = 0$  because varying  $\Omega$  would not change the mass distributions by more than a few percents. This remark can also be extended to the value of  $\Lambda$ , which has a negligible effect on the lens-model parameters (less than 10%), but a more significant impact on the expected distribution of background sources. As shown in Figs. 7 and 8, the value chosen for  $q_0$  affects the expected distribution of background sources at high redshift as well as the total number counts, especially at faint magnitudes where the main contribution comes from the more distant objects. Roughly speaking, when  $q_0$  changes from 0.5 to 0 keeping  $\Lambda = 0$ , the efficiency of the cluster-lens given by  $N(z)$  increases by a small factor of less than  $\sim 10\%$  up to  $z \sim 3$ , but it rises dramatically up to a factor of  $\sim 200\%$  at the highest  $z$  (Figs. 4 and 5). The maximum effect on absolute number counts is  $\sim 30\%$  for the faintest bins in magnitude ( $B \sim 27-28$ ). When we change from a matter dominated ( $(q_0, \lambda_0) = (0.5, 0.0)$ ) to a  $\Lambda$  dominated geometry ( $(q_0, \lambda_0) = (0.0, 0.5)$ ) keeping  $\Omega = 1$  ( $\Omega = 2q_0 + 2\lambda_0$ ), the predicted number counts of arcs will increase by 15% even at moderate magnitudes ( $B = 24-25$ ). According to this result, models with  $\lambda_0 > 0$  could reconcile observed with predicted number counts of arcs. The increase in number counts is even higher when we consider models with low values of  $\Omega$ : it attains 40% at the same moderate magnitudes with  $\lambda_0 \sim 0.9$  and  $q_0 < 0$ , but this model is somewhat unrealistic.

#### 4.2. Redshift distribution of arclets

In the cluster A370, the fraction of galaxies at  $z < 1$  is quite small compared to the distribution in A2218 (Fig. 9). This is essentially related to the difference between the redshift of the

two lenses: the magnification of galaxies at  $z < 0.6$  is much less efficient in A370 ( $z_{lens} = 0.37$ ) than in A2218 ( $z_{lens} = 0.17$ ). This is also visible in the spectroscopic redshift survey of A2218 where 50% of the redshifts are smaller than 0.6.

The main discrepancy between predicted and observed  $N(z)$  for arclets is the apparent lack of objects observed at  $z \geq 1$ . A systematic bias in the sample of spectroscopically confirmed arclets may account partly for these missing galaxies. Indeed objects with  $z$  between about 1.2 and 2.2 can be missed in spectroscopic surveys because of the lack of any emission lines in the visible part of the spectrum. For example, in the spectroscopic sample of Ebbels et al. (1997), most of the redshift determinations considered as secure correspond to spectra with an emission line, generally identified with [OII]. This clearly indicates a bias in the spectroscopic sample to redshifts lower than 1.2 or higher than 2.2. About 40% of their sample of arclets remains with no redshift determination and may correspond to galaxies at  $z > 1$ . A more detailed examination of their photometric SEDs might allow to deduce a photometric redshift and to discuss this particular point. Anyway, as far as no well defined and magnitude-limited samples of arclets are studied yet, no direct comparison with our work can be proposed.

Several uncertainties remain in the general problem of modelling galaxy evolution above  $z \simeq 1$  which could also modify the predicted  $N(z)$ . Computing the redshift distribution of gravitational arclets with  $B \leq 24.5$  is in fact equivalent to the distribution of field galaxies up to  $B \simeq 26$  or even fainter after magnification by the cluster. Evolution models are mostly constrained until  $B = 24$ , where spectroscopic data for field galaxies are available (Glazebrook et al. 1995, Cowie et al. 1996). The bulk of the undetected population of

high redshift arclets at  $z \geq 2$  is made by elliptical galaxies and, in this respect, we join the results obtained in previous works about numbers counts (Bruzual & Kron 1980, Tinsley 1980, Guiderdoni & Rocca-Volmerange 1990, Metcalfe et al. 1991, Pozetti et al. 1996). As long as ellipticals form in a single burst, changing their redshift of formation only modifies the expected  $N(z)$  distribution at high- $z$ , but it does not reduce significantly the total excess in number. The introduction in the model of internal absorption by dust or obscuration by intervening matter along the line-of-sight could decrease the counts at high redshifts. We are mostly interested by the  $B$ -band, equivalent to the rest frame  $UV$ -band, where absorption effects are more important. Internal absorption by dust has been explored by Campos and Shanks (1995). Metallicity effects, which are not taken into account in our model (metallicity is assumed to be solar), would act in the opposite way because the  $UV$  luminosity is increased for a lower metallicity (as expected at earlier epochs). The most straightforward way to solve the problem is to break down the hypothesis that ellipticals form in a unique burst. This idea is also supported by the deep HST images (see also a discussion in Baugh et al. 1997), where the distant galaxies seem rather irregular, deviating from the pure elliptical shape assumed here. In a more general way, there is no observational reason to assert that the progenitors of present day galaxies follow the simple evolutionary laws used here, and the first results on the arclet sample strongly support this idea. There is more probably a strong relationship between morphology and spectrophotometry, the two aspects being both interdependent and wavelength dependent. In any case, the identification of the distant progenitors of ellipticals remains an exciting challenge.

## 5. Conclusions

We have presented in this paper a detailed model of spectrophotometric evolution of galaxies coupled with a gravitational lens model of clusters of galaxies, aimed at studying the population of arclets. The framework for galaxy evolution has been chosen to fairly reproduce the observed number counts and redshift distribution of field galaxies, using the Bruzual and Charlot code, and most of the standard prescriptions for Hubble types and star formation histories. The interest in applying these calculations to arclets is to use cluster-lenses as filters to select representative populations of distant galaxies at various redshifts. Applying our model to two well studied cluster-lenses (A2218 and A370), with arclets samples selected on deep HST images, we derive the following conclusions and results:

- Detailed models for the cluster-lenses, including galaxy-scale mass components, are absolutely needed to interpret the observed distribution of arcs and arclets in terms of general properties of the background population of galaxies.
- Number counts and redshift distributions of arclets at  $z \leq 1.0$  are correctly predicted by our model. The important population of arclets expected at  $z \geq 1.0$ , which is not observed in spectroscopic surveys, could be reduced using more realistic prescriptions in evolutionary models for galaxies at high redshifts. In particular, elliptical galaxies cannot be

formed in a unique burst, whatever the redshift of formation, except if a strong absorption of the rest-frame  $UV$  is the general case.

- Computing the 2D distributions of arclets in number counts or mean redshift seems to be a promising tool. We propose to use these maps, coupled with a photometric redshift selection when possible, to build up spectroscopic samples of high redshift candidates, which represent top priority targets for spectroscopic observations on 8m-class telescopes.

A good agreement between model and observed absolute number counts can be obtained by a fine tuning parametrization of the evolutionary models for galaxies and/or the cosmological parameters. Observing distant cluster-lenses could help on disentangle the role of pure geometrical effects, giving constraints on the world model, from pure spectromorphological evolution. This paper is the beginning of a study, an example on two single clusters at moderate redshift, but the effort has to be pursued on a complete sample of lenses in order to minimize the fluctuations and possible clustering along the line of sight, which is difficult to avoid.

*Acknowledgements.* We thank P'tit Lu Van Waerbeke, J.P. Kneib, Y. Mellier and G. Bruzual for useful discussions and helpful comments. We are especially grateful to B. Fort for a careful reading of the paper and constructive remarks. This work was partly supported by the Groupe de Recherche Cosmologie and by the French Centre National de la Recherche Scientifique.

## References

- Allen S.W., Fabian A.C., Kneib J.-P., 1996, MNRAS, 279, 615  
 Babul A. & Ferguson H.C. 1996, ApJ 458, 100  
 Bartelmann M. & Weiss A., 1994, A&A, 287, 1  
 Bartelmann M., Steinmetz M., Weiss A., 1995, A&A, 297, 1  
 Baugh C.M., Cole S., Frenk C.S., Lacey C.G., 1997, preprint astro-ph/9703111  
 Bertin E. & Arnouts S., 1996, A&AS, 117, 393  
 Bézecourt J. & Soucail G., 1997, A&A, 317, 661  
 Broadhurst T.J., Ellis R.S., Glazebrook K. 1992, Nature, 355, 55  
 Broadhurst T.J., 1995, preprint astro-ph/9511150  
 Brunner R.J., Connolly A.J., Szalay A.S., 1997, astro-ph/9703058  
 Bruzual A.G. & Kron R.G., 1980, ApJ, 241, 25  
 Bruzual G.A. & Charlot S., 1993, ApJ, 405, 538  
 Campos A. & Shanks T., 1995, preprint astro-ph/9511110  
 Connolly A.J., Csabai I., Szalay A.S., 1995, AJ 110, 2655  
 Cowie L.L., Songaila A., Hu E.M., Cohen J.G., 1996, AJ, 112, 839  
 Crampton D., Le Fèvre O., Lilly S.J., Hammer F., 1995, ApJ, 455, 96  
 Ebbels T.M.D., Le Borgne J.F., Pelló R., Kneib J.-P., Smail I.R., Sanahuja B., 1996, MNRAS 281, L75  
 Ebbels T.M.D., Ellis, R.S., Kneib J.-P., Le Borgne J.F., Pelló R., Smail I.R., Sanahuja B., 1997, MNRAS submitted, preprint astro-ph/9703169  
 Efstathiou G., Ellis R.S., Peterson B.A., 1988, MNRAS, 232, 431  
 Ellis R.S., 1997, ARAA, 35, in press  
 Ellis R.S., Allington-Smith J., Smail I., 1991, MNRAS, 249, 184  
 Ellis R.S., Colless M., Broadhurst T., Heyl J., Glazebrook K., 1996, MNRAS, 280, 235  
 Fall S.M., Charlot S., Pei Y., 1996, ApJ 464, L43  
 Fort B. & Mellier Y., 1994, A&AR, 5, 239

- Fort B., Mellier Y., Dantel–Fort M., 1997, *A&A*, 321, 353
- Franx M., Illingworth G.D., Kelson D.D., van Dokkum P.G., Tran K.-V., 1997. preprint astro-ph/9704090
- Fukugita M., Shimasaku K., Ichikawa T. 1995, *PASP* 716, 945
- Glazebrook K., Ellis R., Colless M., Broadhurst T., Allington–Smith J., Tanvir N., 1995, *MNRAS*, 273, 157
- Grossman S.A. & Saha P., 1994, *ApJ* 431, 74
- Guiderdoni B. & Rocca–Volmerange B., 1990, *A&A*, 227, 362
- Hammer F., 1991, *ApJ*, 383, 66
- Hattori M., Watanabe K., Yamashita K., 1997, *A&A*, 319, 764
- Kassiola A. & Kovner I., 1993, *ApJ* 417, 450
- King I.R., 1978, *ApJ*, 222, 1
- Kneib J.–P., Mellier Y., Fort B., Mathez G., 1993, *A&A*, 273, 367
- Kneib J.–P., Mathez G., Fort B., Mellier Y., Soucaïl G., Longaretti P.–Y., 1994a, *A&A*, 286, 701
- Kneib J.–P., Melnick J., Gopal–Krishna, 1994b, *A&A*, 290, L25
- Kneib J.–P., Mellier Y., Pelló R., Miralda–Escudé J., Le Borgne J.F., Böhringer H., Picat J.–P., 1995, *A&A*, 303, 27
- Kneib J.–P., Ellis R.S., Smail I., Couch W.J., Sharples R.M., 1996, *ApJ*, 471, 643
- Koo D.C. & Kron R.G., 1992, *ARAA*, 30, 613
- Kruit P.C. van der, 1987, *A&A*, 173, 59
- Lavery R.J., Pierce M.J., McClure R.D., 1993, *ApJ*, 418, 43
- Le Borgne J.–F., Pelló R., Sanahuja B., 1992, *A&AS*, 95, 87
- Lilly S.J., Tresse L., Hammer F., Crampton D., Le Fèvre O., 1995, *ApJ*, 455, 108
- Lowenthal J.D., Koo D.C., Guzmán R., Gallego J., Phillips A.C., Faber S.M., Vogt N.P., Illingworth G.D., Gronwall C., 1997, *ApJ* 481, 673
- Madau P., 1996, *Cosmic Star Formation History*, in *Star Formation Near and Far*, S.S. Holt & G.L. Mundy eds. (AIP: New York), 481, preprint astro-ph/9612157
- Madau P., Pozzetti L., Dickinson M. 1997, *ApJ* in press, astro-ph/9708220
- Mathewson D.S., Ford V.L., Buchhorn M., 1992, *ApJS*, 81, 413
- Mellier Y., Soucaïl G., Fort B., Mathez G., 1988, *A&A*, 199, 13
- Mellier Y., Fort B., Soucaïl G., Mathez G., Cailloux M., 1991, *ApJ*, 380, 334
- Melnick J., Altieri B., Gopal–Krishna, Giraud E., 1993, *A&A*, 271, L5
- Metcalfe N., Shanks T., Fong R., Jones L.R., 1991, *MNRAS*, 249, 498
- Metcalfe N., Shanks T., Campos A., Fong R., Gardner J.P. 1996, *Nature* 383, 236.
- Mutz S.B., Windhorst R.A., Schmidtke P.C., Pascarelle S., Griffiths R.E., Ratnatunga K.U., Casertani S., Im M., Ellis R.S., Glazebrook K., Green R.F., Sarajedini V.L., 1994, *ApJ*, 434, L55
- Narayan R. & Bartelmann M., 1996, *Lectures on gravitational lensing*, Jerusalem
- Nemiroff R.J. & Dekel A., 1989, *ApJ*, 344, 51
- Pei Y.C. & Fall S.M., 1995, *ApJ*, 454, 69
- Pelló R., Le Borgne J.F., Soucaïl G., Mellier Y., Sanahuja B., 1991, *ApJ*, 366, 405
- Pelló R., Le Borgne J.F., Sanahuja B., Mathez G., Fort B., 1992, *A&A*, 266, 6
- Pelló R., Miralles J.M., Le Borgne J.F., Picat J.P., Soucaïl G., Bruzual G., 1996, *A&A*, 314, 73
- Pozzetti L., Bruzual G.A., Zamorani G., 1996, *MNRAS*, 281, 953
- Pozzetti L., Madau P., Zamorani G., Ferguson H., Bruzual G.A., 1997, *MNRAS* submitted
- Refregier A. & Loeb A., 1997, *ApJ*, 478, 476
- Rocca–Volmerange B. & Guiderdoni B., 1990, *MNRAS*, 247, 166
- Salpeter E.E., 1955, *ApJ*, 121, 161
- Scalo J.M., 1986, *Fund. Cosmic Phys.*, 11, 1
- Soucaïl G., Mellier Y., Fort B., Mathez G., Cailloux M., 1988, *A&A*, 191, L19
- Smail I., Ellis R.S., Fitchett M.J., Nørgaard–Nielsen H.U., Hansen L., Jørgensen H.E., *MNRAS*, 1991, 252, 19
- Smail I., Couch W.J., Ellis R.S., Sharples R.M., 1995, *ApJ*, 440, 501
- Smail I., Dressler A., Kneib J.–P., Ellis R., Couch W.J., Sharples R.M., Oemler A., Butcher H.R., 1996, *ApJ*, 469, 508
- Steidel C., Giavalisco M., Pettini M., Dickinson M., Adelberger K., 1996a, *ApJ*, 462, L17
- Steidel C.C., Giavalisco M., Dickinson M., Adelberger K., 1996b, *AJ* 112, 352
- Tinsley B.M., 1980, *ApJ*, 241, 41
- Trager S.C., Faber S.M., Dressler A., Oemler A., 1997, *ApJ*, 485, 92
- White S.D.M., Frenk C.S. 1991, *ApJ* 379, 25
- Williams R.E., Blacker B., Dickinson M., Van Dyke Dixon W., Ferguson H.C., Fruchter A.S., Giavalisco M., Gilliland R.L., Heyer I., Katsanis R., Levay Z., Lucas R.A., McElroy D.B., Petro L., Postman M., Adorf H.–M., Hook R.N., 1996, *AJ*, 112, 1335
- Wu X.P. & Hammer F., 1993, *MNRAS*, 262, 187